

HARP/ACSIS: A submillimetre spectral imaging system on the James Clerk Maxwell Telescope

J. V. Buckle^{1*}, R. E. Hills^{1,2}, H. Smith¹, W. R. F. Dent^{3,2}, G. Bell¹, E. I. Curtis¹, R. Dace¹, H. Gibson¹, S. F. Graves¹, J. Leech^{1,4†}, J. S. Richer¹, R. Williamson^{1‡}, S. Withington¹, G. Yassin^{1†}, R. Bennett³, P. Hastings³, I. Laidlaw³, J. F. Lightfoot³, T. Burgess⁵, P. E. Dewdney⁵, G. Hovey⁵, A. G. Willis⁵, R. Redman⁶, B. Wooff⁶, D.S. Berry⁴, B. Cavanagh⁴, G.R. Davis⁴, J. Dempsey⁴, P. Friberg⁴, T. Jenness⁴, R. Kackley⁴, N. P. Rees^{4§}, R. Tilanus⁴, C. Walther⁴, W. Zwart⁴, T. M. Klapwijk⁷, M. Kroug⁷, T. Zijlstra⁷

¹*Cavendish Astrophysics Group, Cavendish Laboratory, University of Cambridge, J J Thomson Ave., Cambridge CB3 0HE, UK*

²*ALMA JAO, Av. El Golf 40 - Piso 18, Las Condes, Santiago, Chile*

³*UK Astronomy Technology Centre, Blackford Hill, Edinburgh, EH9 3HJ, UK*

⁴*Joint Astronomy Centre, 660 N. A'ohoku Place, Hilo, HI, 96720, USA*

⁵*Dominion Radio Astrophysical Observatory, PO Box 248, White Lake*

⁶*Herzberg Institute of Astrophysics, 5071 West Saanich Road, Victoria, BC, V9E2E7, Canada*

⁷*Delft University of Technology, Faculty of Applied Sciences, Kavli Institute of Nanoscience, Lorentzweg 1, 2628 CJ Delft, The Netherlands*

ABSTRACT

This paper describes a new Heterodyne Array Receiver Programme (HARP) and Auto-Correlation Spectral Imaging System (ACSIS) that have recently been installed and commissioned on the James Clerk Maxwell Telescope (JCMT). The 16-element focal-plane array receiver, operating in the submillimetre from 325 to 375 GHz, offers high (three-dimensional) mapping speeds, along with significant improvements over single-detector counterparts in calibration and image quality. Receiver temperatures are ~ 120 K across the whole band and system temperatures of ~ 300 K are reached routinely under good weather conditions. The system includes a single-sideband filter so these are SSB figures. Used in conjunction with ACSIS, the system can produce large-scale maps rapidly, in one or more frequency settings, at high spatial and spectral resolution. Fully-sampled maps of size 1 square degree can be observed in under 1 hour.

The scientific need for array receivers arises from the requirement for programmes to study samples of objects of statistically significant size, in large-scale unbiased surveys of galactic and extra-galactic regions. Along with morphological information, the new spectral imaging system can be used to study the physical and chemical properties of regions of interest. Its three-dimensional imaging capabilities are critical for research into turbulence and dynamics. In addition, HARP/ACSIS will provide highly complementary science programmes to wide-field continuum studies, and produce the essential preparatory work for submillimetre interferometers such as the SMA and ALMA.

Key words: instrumentation: detectors – instrumentation: spectrographs – methods: observational – techniques: image processing – techniques: spectroscopic – submillimetre

* E-mail: j.buckle@mrao.cam.ac.uk

† Present address: Oxford Astrophysics Group, Denys Wilkinson Building, Keble Road, Oxford, OX1 3RH

‡ Present address: Department of Astronomy, Columbia University, Pupin

Physics Laboratories, 550 West 120th Street, New York, New York 10027, USA

§ Present address: Diamond Light Source Ltd, Harwell Science and Innovation Campus, Oxfordshire, OX11 0DE

1 INTRODUCTION

The James Clerk Maxwell Telescope (JCMT), situated on a high, dry site near the summit of Mauna Kea, and with a 15 m dish, is the largest submillimetre observatory in the world. The submillimetre band is rich in molecular lines, and so high-resolution spectroscopy at these wavelengths enables studies of space densities, velocities, chemical structure and excitation in the gaseous material of both galactic and extra-galactic sources. The majority of these sources are extended on scales larger than the JCMT beam size of ~ 14 arcsec (at 345 GHz), and many astronomical targets are much larger, extended on parsec scales, which frequently need to be mapped to carry out relevant astronomical research. With submillimetre heterodyne receivers approaching background-limited performance, the scientific need for focal-plane heterodyne array receivers is clear. By building multiple detectors, mapping speeds can be increased, making possible programmes which observe samples of objects of useful statistical size.

HARP (Heterodyne Array Receiver Programme) and ACSIS (Auto-Correlation Spectral Imaging System) have recently been installed and commissioned on the JCMT. HARP operates in the submillimetre band spanning 325 to 375 GHz, a frequency range which contains transitions from nearly all the most abundant molecules in interstellar gas. The key scientific programmes that are expected to be carried out with the new system are

- surveys of the distribution and properties of molecular clouds in face-on and edge-on galactic disks, starburst and Seyfert galaxies, and interacting galaxy systems;
- large-scale unbiased surveys of star formation and outflows in molecular clouds;
- large-scale studies of hierarchical structure and clumping in molecular clouds;
- studies of the chemical processing of molecular clouds by shocks and turbulence;
- surveys of the dynamics and excitation of molecular gas in the Galactic centre;
- deep, narrow surveys of molecular gas in Solar System objects;
- studies of the chemical and physical state of comets near perihelion.

Several large JCMT legacy survey projects have been developed to exploit this new instrumentation in the above scientific areas (Ward-Thompson et al. 2007; Plume et al. 2007; Matthews et al. 2007; Wilson et al. 2009). The combination of HARP and ACSIS makes possible science which is highly complementary to the wide-field continuum studies of cold dust in distant galaxies and the earliest stages of star formation that have been carried out by SCUBA (Holland et al. 1999), and will continue with SCUBA-2 (Holland et al. 2006). It will also provide the essential scientific preparatory work for submillimetre interferometers such as the SMA and ALMA.

In addition to the increase in mapping speeds, HARP/ACIS offers supplemental benefits, the most important of which is probably the decrease in calibration errors and increase in image quality, since multiple detectors observe the source simultaneously. Relative calibration of individual detectors is more accurate, as data are taken simultaneously through the same atmospheric path. By making overlapping maps, pointing drifts between maps can be removed. For objects smaller than the array field of view, edge detectors can be used to make reference spectra through on-array beam

switching by using appropriately selected chop and node distances, thereby increasing the mapping speed of compact objects.

The full ACSIS capabilities are described in Sec. 3. When used with HARP, ACSIS offers either wide bandwidths (up to ~ 1.9 GHz for each of the 16 IF channels), or high spectral resolution (with a channel spacing as small as 31 kHz, or 0.03 km s^{-1}). In addition, it can provide one or two sub-bands per IF channel, allowing simultaneous observations of multiple lines within the HARP 5 GHz IF frequency. One example is observing the $J=3 \rightarrow 2$ lines of ^{13}CO and C^{18}O with two separate high-resolution sub-bands. ACSIS and the upgraded JCMT Observatory Control System allow for rapid observing and data taking. Fast scanning enables data to be taken continuously at up to 10 Hz, and it is possible to make fully-sampled maps with HARP of 1 square degree in less than 1 hour.

As shown in Fig. 1, HARP has been installed on the right-hand Nasmyth platform of the JCMT. An optical relay (Fig. 2) provides the field of view and imaging performance to match the HARP specifications. The relay optics also bring the beam down to a lower level so that the cryostat is conveniently accessible on the Nasmyth platform. A schematic diagram of the components of HARP is shown in Fig. 3. The path is further explained in Sec. 2.2. Each of the components is described in the following sections, with Sec. 2 describing the HARP components, and Sec. 3 describing the ACSIS components.

Designing and building HARP was a collaborative project between the Cavendish Astrophysics Group in Cambridge, the UK Astronomy Technology Centre in Edinburgh, the Herzberg Institute for Astronomy in Victoria, Canada, and the Joint Astronomy Centre in Hawaii, with the Kavli Institute of Nanoscience at Delft contributing the critical SIS junctions. ACSIS was built in collaboration between the Dominion Radio Astrophysical Observatory in Penticton, Canada, the UK Astronomy Technology Centre and the Joint Astronomy Centre.

2 HARP DESIGN CONCEPTS

A description of the key design features of the instrument, along with technical and organisational overviews, have previously been published (Smith et al. 2003, 2008). In this section we present a brief overview of the key features of HARP's specification, design and performance.

2.1 Overview

HARP comprises 16 detectors laid out on a 4×4 grid, with an on-sky projected beam separation of 30 arcsec. At 345 GHz the beam size is 14 arcsec, and the under-sampled field of view of HARP is 104×104 arcsec, as shown in Fig. 4. In a single pointed observation, the map is under-sampled by a factor of 4.4 in area, and by a factor of 17.6 with respect to the Nyquist frequency ($\lambda/2D$).

Beam rotation, using a new K-mirror (Sec. 2.2.1), optimizes the observing efficiency. For objects similar to or smaller than the array field of view, beam rotation ensures no edge detectors miss the source emission. For larger objects, and particularly for scan mapping, the array can be orientated with respect to the scan direction to provide good sampling (Sec. 4). HARP is easily and rapidly tuned across the operating range of 325 to 375 GHz using automated control software in 10–30 seconds (Sec. 3.4). The IF frequency is 5 GHz, and, in conjunction with ACSIS, HARP offers up to 1.9 GHz of bandwidth.

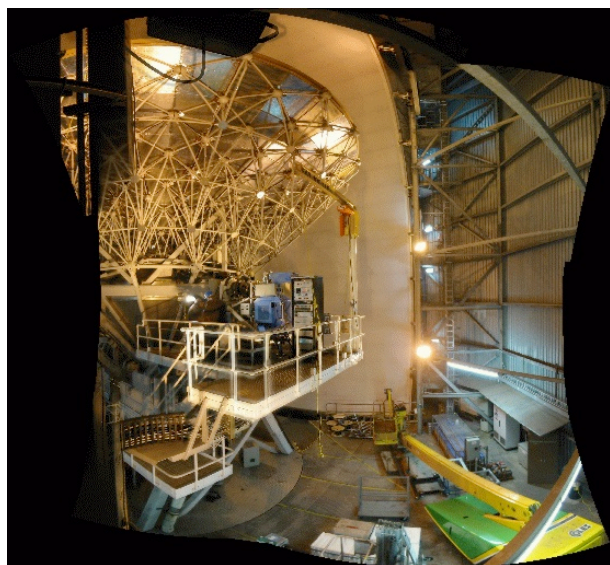


Figure 1. HARP shown on the right-hand Nasmyth platform of the JCMT, and a zoomed-in image of HARP and the instrument electronics box.

HARP uses single sideband (SSB) filtering to minimize the system temperatures and improve calibration accuracy. HARP sensitivities have exceeded expectation, with the combination of receiver noise temperature and beam efficiency better than the required 330 K (SSB). Relative inter-receptor calibration, measured on continuum sources, is accurate to better than 5 per cent, and relative beam positions can be measured to an accuracy of 1 arcsec.

HARP utilizes a number of innovative features across all elements of the design. The key features of these are outlined below. Further technical details and schematic diagrams are presented

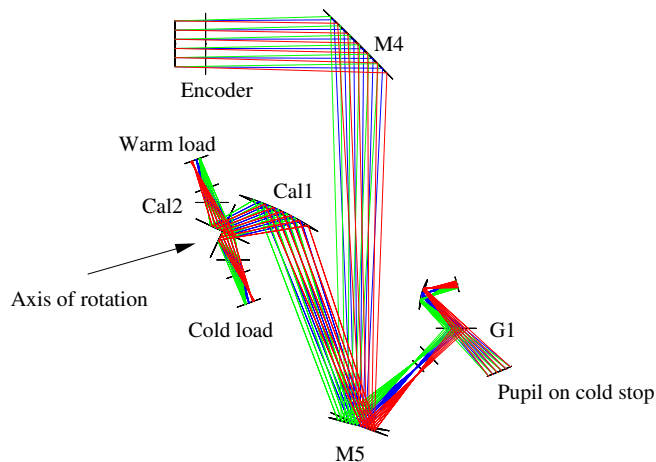


Figure 2. Diagram of the relay optics from the encoder to the cold stop, through a series of labelled mirrors.

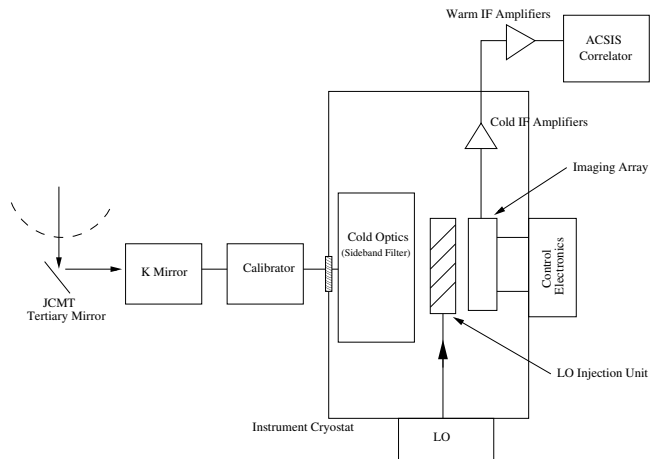


Figure 3. A schematic diagram of the components of the HARP receiver system, adapted from Leech (2000).

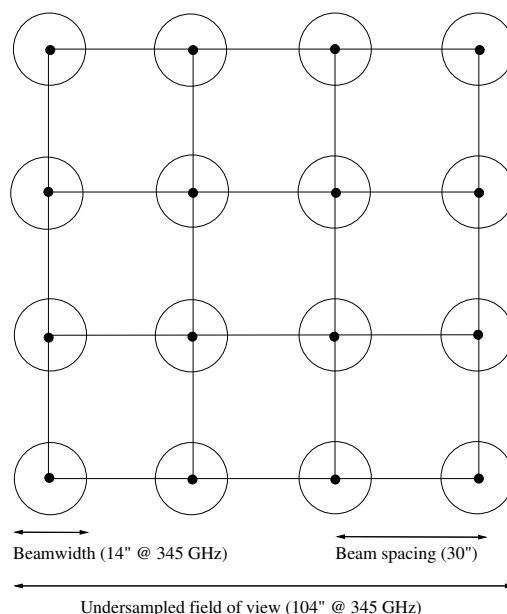


Figure 4. Schematic diagram of the HARP grid layout.

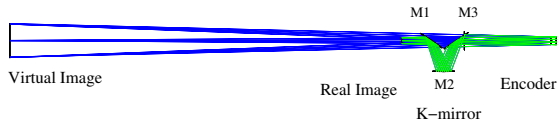


Figure 5. Schematic of the K-mirror, showing the three mirrors, M1 to M3. The JCMT tertiary mirror is just to the left of the real image.

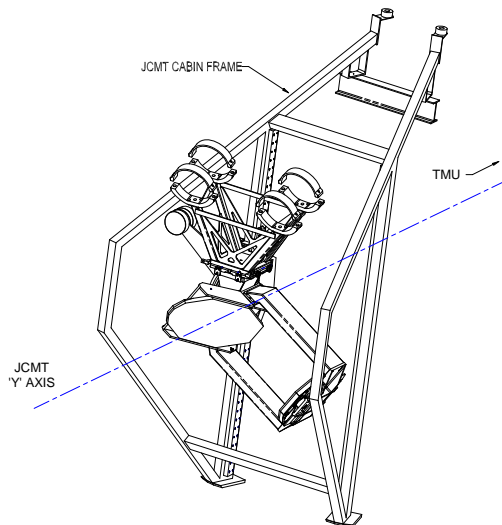


Figure 6. Schematic overview of the K-mirror in the JCMT receiver cabin. The JCMT ‘Y’ axis is the elevation axis.

elsewhere (Smith et al. 2003; Leech 2000; Williamson 2004; Smith et al. 2008; Bell 2008).

2.2 Optical system

The optical system for HARP has three sections. The K-mirror is inside the receiver cabin and described in Sec. 2.2.1. The warm optics, comprised of the relay optics and calibration system, are exposed on the Nasmyth platform, and are described in Sec. 2.2.2. The cold optics are contained inside the cryostat, and are described in Sec. 2.2.3.

2.2.1 K-mirror

The K-mirror (Fig. 5) consists of three large powered mirrors with modest curvature. The system acts as an image and polarization rotator, and forms an image of the secondary mirror at a point near the elevation encoder. An overview of the K-mirror in the JCMT receiver cabin is shown in Fig. 6. The K-mirror also maximizes the field of view available to instruments on the Nasmyth platform, which otherwise would be severely limited due to the relatively small hole in the encoder axis. The K-mirror rotates as a unit about the elevation axis of the telescope, and has a rotational range of ± 57.5 degrees, limited through control software to ± 55 degrees, with the effective rotation of the image and polarization twice the K-mirror rotation angle. The K-mirror can rotate at a rate of 5 degrees s^{-1} , with a rotational position accuracy of ± 0.1 degree. The design allows for a field of view of ~ 200 arcsec. The system is designed to have very low losses and aberrations. Spillover loss is designed to be less than 1 per cent, and in fact is expected to be < 0.5 per cent at $850 \mu m$. The losses per mirror should be less than

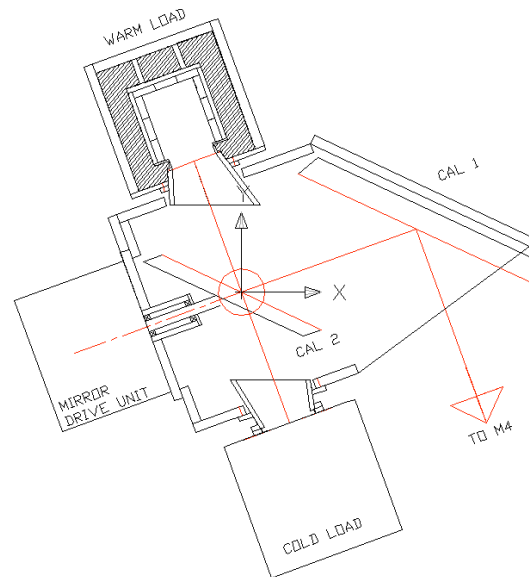


Figure 7. The calibration system (from Williamson 2004).

0.5 per cent at this wavelength, which will contribute ~ 3 K to the system temperature from each mirror. In order to meet the needs of possible future JCMT instrumentation, the mirror surfaces have been finished so that they are compatible with the highest operational frequencies at the JCMT of ~ 870 GHz.

Rotation of the K-mirror is controlled by the Telescope Control System (TCS). The TCS commands a continuous rotation of the K-mirror to compensate for the change in parallactic angle of the source and the rotation of the elevation axis of the telescope. When the telescope is commanded to slew to a new position, the TCS computes an optimal orientation of the focal plane relative to the tracking coordinate system to give the longest tracking time on source before hitting one of the K-mirror rotation limits. This optimal orientation corresponds to an initial K-mirror angle to which it is slewed and then the TCS continuously updates the angle to maintain a fixed orientation between the focal plane and tracking coordinate systems throughout the observation.

The pointing offsets due to possible misalignment of the K-mirror axis and its axis of rotation have been calculated, and included in the JCMT pointing model. The effective pointing of the telescope on the sky is changed if the mirrors are displaced or tilted, so a requirement of the K-mirror is that total pointing errors are less than 10 arcsec. Residual pointing errors, after subtraction of the known correction terms, are a few arcsec, partly due to the number of new terms in the pointing model introduced by the K-mirror.

2.2.2 Calibration

A schematic overview of the calibration system is shown in Fig. 7. The calibration unit was built as an independently mounted unit containing the two mirrors, Cal1 and Cal2, the warm and cold loads, and a spectral-line calibration signal (Fig. 2). Cal1 is strongly concave and fixed, while Cal2 is flat, and can turn from the warm load to the cold load in under 2 s. The loads are isothermal cuboid cavities lined with absorbing tiles that have high efficiency at the HARP operational frequencies. A thermally isolated conical reflecting baffle at the input limits the IR coupling. The positions of the loads were chosen to minimize convection.

To make calibration measurements, a lower relay mirror (M5,

Fig. 2) is tilted mechanically to point to the calibrator unit, where the Cal2 mirror focuses the beams on to either the warm or cold load. The Cal2 mirror is actuated by a standard four-position ‘‘Geneva’’ mechanism, while the M5 mirror is actuated by a novel Geneva design of a two-position type. The Cal1 mirror then rotates to switch between the loads. The warm load is heated by resistors to temperatures ~ 40 K above ambient. The cold load is cooled to ~ 10 K below ambient temperatures using a Peltier cooler, with the intention of providing a load that is at approximately the same temperature as the water vapour in the atmosphere. Two- or three-load calibration measurements can be taken in a few seconds. A two-load calibration, which measures the power from the sky and the power from the cold load, should then accurately remove atmospheric attenuation. The three-load calibration, which additionally measures the power from the warm load, provides a measure of the receiver temperature.

The Cal2 mirror has a third position which allows it to point at the spectral-line calibration signal. This coherent signal is used to check the tuning of the interferometer (Sec. 2.2.3) and to optimize the signal-to-noise ratio when adjusting tuning parameters such as the bias voltage and local oscillator (LO) level. It uses a YIG oscillator and a multiplier to produce a narrow line which can be tuned to lie anywhere in the HARP operational frequency range. The optics are arranged to couple this signal into all the mixers at the same time with a reasonable degree of uniformity.

The night-to-night calibration accuracy has been measured to be within JCMT guidelines of 20 per cent, and is usually better than this (Sec. 5.4). Work on improving the accuracy and stability of the combined HARP, ACSIS, telescope and software systems continues at the JCMT. The receptor-to-receptor calibration accuracy was measured with observations on the nearly full Moon (Fig. 18), and indicate maximum differences between levels less than 5 per cent. Any variation of calibration with ambient temperature is at levels below both the night-to-night and receptor-to-receptor calibration accuracy.

2.2.3 Cold optics

The cold optics are located inside the cryostat, and operate at temperatures ~ 60 K. Four powered mirrors (Fig. 8) between the encoder and the array are optimized together to take advantage of aberration balancing. Utilizing a reflective, slightly curved cold stop inside the cryostat, the system forms an image of the sky with low aberration at the detector array. The smallest mirror, C1, forms the cold stop, while C2F and C2M create an image of the sky at the mixer array.

A polarizing Mach-Zehnder interferometer is used for the sideband separation and the image sideband is terminated in a cold load, inside the cryostat. C2M is moved to tune the interferometer, and the full range of movement for this tuning can be achieved in under 10 s. The HARP IF frequency of 5 GHz sets the path difference requirement for the two beams through the interferometer of 15 mm. Leakage and cross talk levels between the beams were looked for during on-sky commissioning, and were not detected at the 1 per cent level.

The interferometer is tuned so that the path difference is a whole number of wavelengths for the image frequency. This means that the path difference of the signal frequency, once it has completed transmission through the system, is an odd number of half-wavelengths. This results in the signal in the desired sideband being coupled to the mixers and in the other sideband the mixers are coupled to the SSB load. The tuning range achieved covers 324 GHz to

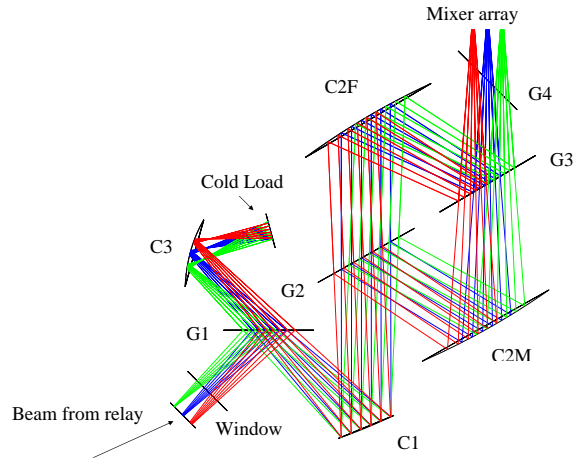


Figure 8. Overview of the cold optics, showing the four mirrors (Cn) and the four grids (Gn) of the polarizing Mach-Zehnder interferometer.

376 GHz. The grids are made from gold-plated tungsten wire with diameter $10 \mu\text{m}$ and spacing $25 \mu\text{m}$. G1 and G4 are rectangular, while G2 and G3 are circular. The two sets of grids are aligned to split the signals into ± 45 degree components. The image sideband dump provides a termination for the beam transmitted through G1, and consists of a concentrator mirror, C3, which operates at ~ 60 K, and a thermally-isolated cold load (the SSB load), which is cooled to ~ 12 K. The details of the design and laboratory testing of the cold optics systems are fully explained in Williamson (2004) and Bell (2008).

The reflective cold stop, C1 is surrounded by cold absorber, which is typically at 18 K. The cold optics also truncate the sidelobes of the feed pattern, so they see cold absorber inside the cryostat rather than thermal emission from the region around the elevation encoder. The interferometer is the critical item in the cold optics, and provides the datum position to which the other components are referenced, with the cryostat window providing the interface to the rest of the system. Sideband separation commissioning tests were carried out across the observing bandwidth, and were measured to be better than 19 dB on average (Sec. 5).

2.3 Imaging array

The imaging array unit comprises an array of mylar beam splitters for LO injection, two decks of eight horn-reflector antennas holding 16 SIS mixers with air-cored coils for Josephson current suppression, and 16 HEMT cold IF amplifiers with isolators and bias tees (a T-shaped multiplexer). The horn reflector antennas consist of split-block, directly machined corrugated horns with ellipsoidal reflectors. The corrugated horns were designed to be easy to mass produce using direct machining into a split block. The novel horn design features constant depth corrugations and delivers good beam patterns across the required bandwidth while avoiding difficult to machine $\sim \lambda/2$ deep corrugations near the throat of the horn. Ellipsoidal reflectors were chosen to provide efficient coupling of the horns to both the telescope fore-optics and the LO meander line. The imaging array unit is shown schematically in Fig. 9. The array is mounted inside the 20 K heat shield.

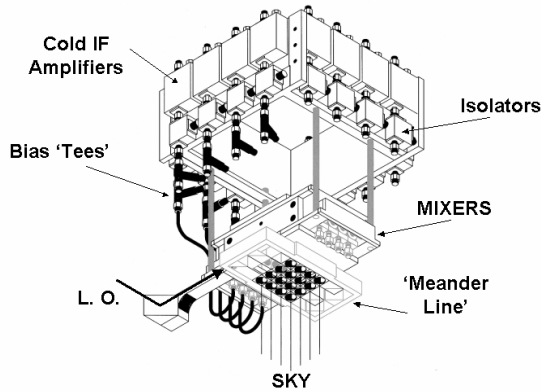


Figure 9. The HARP imaging array.

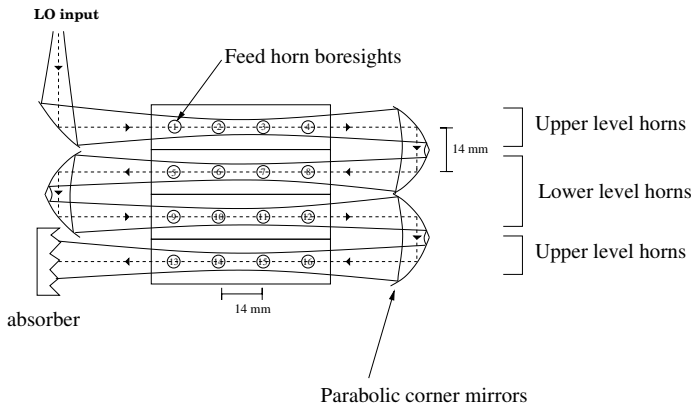


Figure 10. Plan view of the LO coupler.

2.3.1 The local oscillator coupler

The LO coupler uses a ‘meander line’ to provide the efficient coupling necessary to pump 16 mixers (Fig. 10). At each crossing point there is a 45 degree beam-splitter made of thin mylar film. The mylar in the beam-splitters was pre-tensioned to ensure it remains tight when cooled. In order to prevent the beam from diverging due to diffraction as it passes through the meander line, the roof mirrors that are used to turn the beam around after passing in front of each set of 4 mixers consist of off-axis paraboids. These produce beam waists at the mid-points of each path. This arrangement has a large RF bandwidth, and injects LO power in a highly efficient manner (Leech 2000).

For ease of maintenance and upgrades, this unit is independent of the cold optics, with the LO plate mounted on the door of the cryostat. The LO is generated outside the cryostat (Fig. 3), and injected into it through a small polypropylene window. To minimize adjustments with the operational system, a relatively slow beam is generated with optics on the LO plate, which is refocused with a mirror attached to the array unit before it enters the meander line. To provide the correct polarization, two mirrors are used on the LO plate. A small relay consisting of flat and off-axis paraboloid mirrors outside the cryostat and a further small paraboloid mirror inside the cryostat carries the beam from the horn on the LO plate

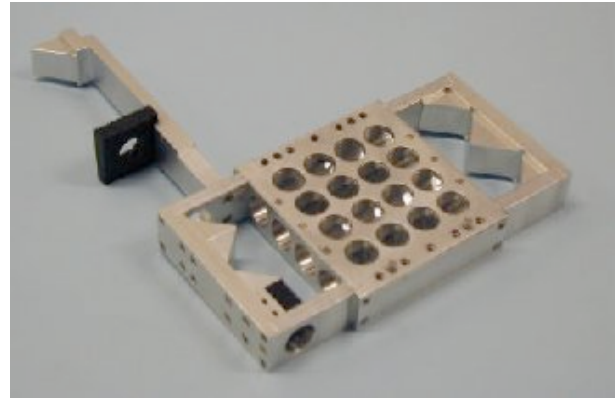


Figure 11. Photograph of the assembled LO coupler, also showing one mirror of the LO relay and the stop.

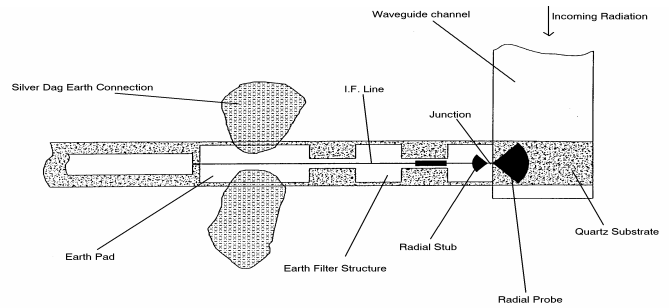


Figure 13. Overview of the radial probe SIS mixer devices.

to the LO coupler. The adjustment to bring the LO beam into alignment is accomplished using pusher screws to tilt and shift the two mirrors. The LO coupler is machined from aluminium. The stop is a 12 mm hole in an absorbing plate which is used to clean up the beam (Fig. 11). Diagnostics are provided by observing the pumped I/V curves on the mixers to obtain as uniform a distribution of LO power as possible. An image of the I/V and P(IF)/V curves displayed by the HARP control software during operation is shown in Fig. 12.

2.3.2 Radial probe mixers

The radial-probe SIS mixers were designed and developed at the Cavendish Astrophysics Group (Leech 2000; Withington et al. 2001) and fabricated in the Kavli Institute of Nanoscience at Delft. The design, shown in Fig. 13, gives extremely broadband operation with similar characteristics for each device. A single-sided radial probe couples power from the rectangular waveguide to the SIS junction. These radial probes have been shown, using scale model experiments and modelling, to give a good impedance match to typical SIS junctions (Leech 2000; Kooi et al. 2001). The capacitance of the SIS junction is tuned out using an inductive microstrip stub end loaded with a radial stub to present a short circuit at the end of the microstrip.

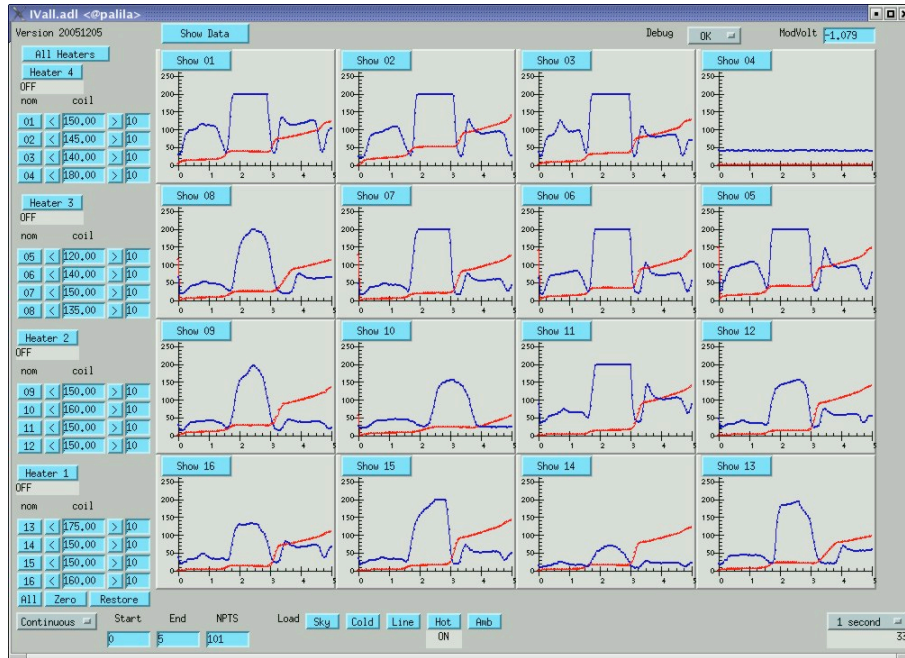


Figure 12. The HARP control system I/V and P(IF)/V curves display.

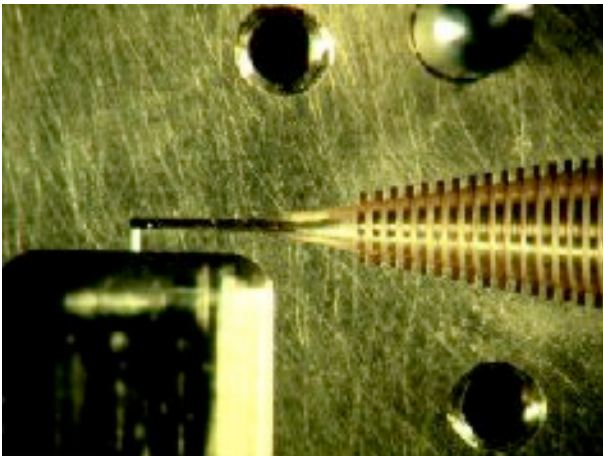


Figure 14. Photograph of the HARP horn near the throat, demonstrating the excellent machining quality. The grooves on the horn have a width of 0.1 ± 0.01 mm.

The imaging receptor is based on the horn-reflector antenna – each mixer consists of a corrugated waveguide horn with a reflector mirror at its aperture. The feed-horn, waveguide, device and IF slots which form the mixer were manufactured as split aluminium blocks, then gold-sputtered. This gives blocks that are lightweight, low thermal mass, free from waveguide flanges and straight-forward to machine. A photograph of one of the finished HARP horns is shown in Fig. 14.

One problem that can arise is the unwanted movement of trapped magnetic flux near the SIS junctions. Typically the unwanted Josephson tunnelling of Cooper pairs is suppressed using a coil to apply a specific strength of magnetic field across the SIS junction. Unfortunately, quantized vortices of magnetic flux, usually trapped by defects in the superconducting film near the SIS junction, can move around under the influence of external electro-

magnetic fields. If these vortices are close to the SIS junction, this can result in a change of the magnetic field applied to it. The magnetic field is then no longer at the value needed for supercurrent suppression and Cooper pairs begin to tunnel, leading to increased noise and decreased stability in the mixer. With large arrays, the movement of trapped flux is potentially a major problem, and one of the reasons why mixers require different amounts of LO power to achieve optimum performance. In HARP, the mixers feature arrays of tiny holes in the niobium (Nb) film near the SIS junction to prevent the movement of trapped flux (Leech 2000). If trapped flux is still proving problematic, small resistive heaters can be used to briefly raise the array above the critical temperature for Nb, destroying the trapped flux vortices. As a routine start up procedure, the telescope operator runs the ‘all heaters’ command (top left of the image in Fig. 12), which briefly warms the array. While this process is occurring, the changes to the I/V and P(IF)/V curves can be monitored in real time. For more localized problems, individual heaters can be used on 4 of the detectors at a time. The control software screen shown in Fig. 12 is thus an extremely useful diagnostic tool, and can be used to check the status and stability of the HARP mixers throughout an observing run.

2.3.3 IF system

The IF system for each receptor consists of a bias tee, isolator and cold IF amplifier connected to the 4 K stage, and two warm IF amplifiers separated by a bandpass filter and a fixed level setting attenuator mounted outside of the cryostat (Fig. 9). The co-axial interconnecting cable from the 4 K stage to the wall of the cryostat is made of stainless steel to minimize the heat load on the 4 K stage. An IF frequency of 5 GHz, with a minimum bandwidth of 1.6 GHz, is used. The overall mid-band gain is a minimum of 57 dB, with a noise temperature ~ 7 K.

3 ACSIS AND OCS DESIGN CONCEPTS

AC SIS consists of IF components and samplers, as well as the correlator hardware and software. ACSIS also includes the initial parts of the data reduction pipeline and the real time data monitoring facility. The signal path is shown in Fig. 15, and described in Sec. 3.1 and Sec. 3.2. The data storage is described elsewhere (Hovey et al. 2000). The overall control of heterodyne observations at the observatory, including HARP, ACSIS and the telescope subsystems, uses real time hardware and software sequencers (Hovey et al. 2002), and is described in Sec. 3.4. In Sec. 3.1–3.3 below, we describe the ACSIS hardware and software.

3.1 IF system

A block diagram showing the IF signal path from the switching network (SWN) is given in Fig. 15. The input IF frequencies cover from 3.3 to 7.7 GHz. There are 16 IF signals feeding from HARP and 8 feeds from additional receivers. Switching between these inputs is done by an IF switch. In addition, a Build In Test Unit (BITE) can also feed white noise (with a 3 dB switchable level) and an optional frequency comb to all ACSIS input channels. Each of the 16 HARP IF inputs can feed at least two Down Converter Modules (DCMs) while each of the 8 non-HARP IF inputs, or equally 8 of the HARP IF inputs, can feed 2 or 4 DCMs. Each DCM extracts a nominal 1 GHz or 0.25 GHz wide band from the 3.3 - 7.7 GHz ACSIS IF band. The frequency range extracted is determined by setting the appropriate second LO (LO2). Four tunable LO2s are fed to each set of four DCMs that can be connected to an IF input. A total of 32 DCMs are available. These 2 or 4 DCMs can be placed anywhere in the ACSIS IF band using the four LO2s. Due to the sharing of LO2s the positioning must be the same in all IF inputs.

As described in Sec. 3.2 ACSIS can combine the correlators attached to adjacent DCMs doubling the number of frequency channels while halving the effective numbers of available DCMs. These basic modes are listed in Table 1.

With the restriction that all IF inputs are configured identically we can now pick modes until all 32 DCMs are used. For instance for HARP we can chose two 1 GHz bands with 976 kHz resolution or one 1 GHz band with 488.3 kHz resolution. We can also chose one 250 MHz and one 1 GHz with the lower resolution. These setups can be used to observe two lines simultaneously e.g. the $J = 3 \rightarrow 2$ lines of ^{13}CO and C^{18}O - see Sec. 6.1.1. For non-HARP receivers with a maximum of 8 IF inputs we can chose (i) up to four 250 MHz; or (ii) up to four 1 GHz low resolution bands; or (iii) two high resolution bands; or (iv) two low resolution bands and one high resolution band. There are a large number of combinations possible.

Further, the observing preparation software can place these bands so they overlap in frequency space. The spectra are reduced and stored separately but are later merged by the data reduction software forming hybrid bands. The possibilities including the hybrid modes for HARP are summarized in Table 2. In principle, four 1 GHz bands could be combined to form a single 3.7 GHz hybrid spectra for non-HARP receivers, although the current JCMT receivers do not have a usable IF bandwidth as large as this.

In the DCM, each sub-band is amplified, filtered and converted to the sampler frequency range (baseband). The DCMs mix the IF with a tunable LO (LO2). A final LO (LO3) fixed at 2.0 GHz does the final downconversion to the baseband. Rather than having multiple system bandwidth/resolution combinations using many differ-

ent IF filters, the philosophy is to have only two hardware options, and ensure that these cover most astronomical requirements. Each DCM can therefore switch between a wideband (1 GHz) and a narrowband (250 MHz) mode (see Table 1). In practice, the edges of the DCM filtering limits the bandwidth of each DCM to 930 MHz and 220 MHz respectively – these are the worst case, the -3 dB power points of the DCMs. After anti-alias filtering, the total power (TP) signal is measured and the RF signal is then fed through an automatic level control (ALC) circuit. The ALC is used to maintain constant TP into the samplers, in order to ensure the most stable system bandpass (and the flattest baselines), and the optimal digitization threshold. The TP signal is recorded and re-applied to the data stream in the ACSIS real time data reduction. The DCMs use MMIC architecture and miniaturized components, and plug into a standard VME backplane. A second section of the backplane includes SMA “blind-mate” connectors for the RF analogue signals, allowing for simple field replacement of the whole unit. The IF systems are mounted within temperature-controlled racks, using a liquid glycol cooler system and external heat exchanger. On board each DCM unit are temperature probes and a heater for internal temperature control. In this way temperatures within the DCMs are maintained to better than 0.1 K over time-scales of hours. This was done to maintain good passband flatness, particularly in the hybrid configurations. A single VME IF control computer is used to read out TP signals and run the temperature control feedback loop for all 32 DCMs.

3.2 Samplers and correlators

Each DCM output is fed to a single sampler unit, running with a fixed clock speed of 2.0 GHz. In 1 GHz mode this unit digitizes the full bandwidth at the Nyquist frequency, and in 250 MHz mode it Nyquist samples the 500–750 MHz band, aliased down to baseband by only keeping each fourth sample. The sampler uses Sony dual high-speed comparator chips implementing a 3-level sampler. At optimum sampling levels, their quantization noise reduces the correlator efficiency to 0.81 (so the noise in the final spectrum is increased by a factor of 1.23 over a perfect spectrometer). A serial-to-parallel converter on each sampler board provides a parallel digital data stream for connection to the correlator board.

The correlator boards uses the “QUAINT” custom correlator chips (Escoffier 1998), running at a clock speed of 62.5 MHz. The chips were deliberately run at reduced clock rate to reduce heat dissipation down to ~ 1.5 W (especially important with the reduced atmospheric pressure on Mauna Kea) in order to increase lifespan. Each chip has 1024 lags, and 32 chips are mounted on each correlator board. Digitized data at $2.0 \text{ GSamples s}^{-1}$ is stored rapidly on to RAM on each board, and read out in parallel to all 32 correlator chips for processing at the slower clock rate. Thus each board can provide 1024 lags with 1.0 GHz total bandwidth. In 250 MHz mode the digitized data is stored at $0.5 \text{ GSamples s}^{-1}$ allowing four correlator chips to be chained together creating 8 correlators with 4096 channels each per board.

The number of channels can further be increased by only recording the incoming digitized data half the time. The time gained allows more correlator chips to be chained together. Two correlator boards time-interleaved in this fashion will correlate all incoming data with twice the number of effective channels. In practice, to avoid extra switching networks, the IF signal is fed to two DCMs, samplers, and correlator boards, and the lags synchronously read by the two sets of correlator boards.

Data is accumulated in the correlator chips, and all 32 chips on

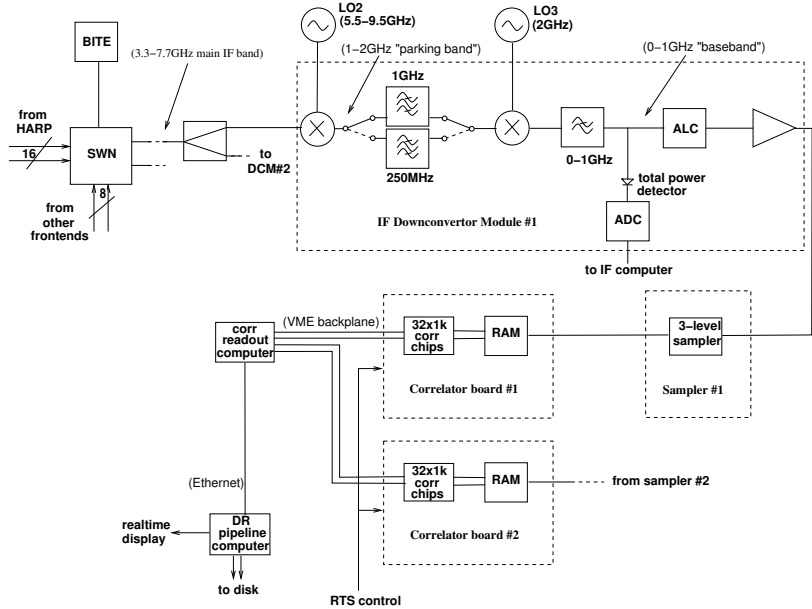


Figure 15. ACSIS overall system hardware block diagram. Only one of the 32 Down Converter Sampler subsections is shown. The signal path is described in the text.

Table 1. ACSIS basic modes.

Nominal bandwidth	Usable bandwidth /MHz	DCMs	Spectral channels	Channel spacing /kHz
250 MHz	~220	1	4096	61.0
1 GHz	~930	1	1024	976.6
250 MHz	~220	2	8192	30.5
1 GHz	~930	2	2048	488.3

each board can be read out to the real time computers every 100 ms to 10 s. Data-taking on the correlator boards (and the TP detector) is controlled through three hardware control bits fed from the Real Time Sequencer (or RTS; see below and Hovey et al. 2002). Each data sample has a unique sequence number (N), used in the later data reduction stages. Each VME real time readout computer is used to read 4 correlator boards, combine the autocorrelation functions (ACF) from the chips which are being used in parallel, and normalize the ACF. The processed data are then transferred to the main data reduction pipeline computers over the Ethernet connection.

3.3 Data reduction system

Data from all eight real time correlator computers plus the IF computer are fed over Gigabit Ethernet to the reduction cluster. This cluster consists of eleven general-purpose computers which use the DRAMA messaging system (Bailey, Farrell & Shortridge 1999) for communication, and run CASA (Jaeger 2008) and Glish for the real time data reduction. Nine of these computers run independent Sync, Reduction and Gridder tasks for reducing the data. The other two run real time display and data storage tasks. The Sync tasks gather relevant data from the observatory subsystem necessary to describe and reduce each data sample (with sequence number N – see Real Time Sequencer section below – and DCM number M). Subsystems which provide data to the Sync tasks include the RTS,

TCS, secondary mirror (SMU), beam rotator, frontend computer, and ACSIS IF and correlator computers. It has internal buffering to allow different subsystems to send data asynchronously, and only sends the data package on to the reduction tasks once all the relevant data are gathered.

The reduction tasks take the data package, multiply the ACF by the IF TP signal for each sequence number N and DCM channel M ($P(N, M)$), Fourier Transform (FT) the ACF and apply a van Vleck correction (D’Addario et al. 1984) to give the total power spectrum ($S(N, \nu)$) for each data sample and DCM channel being used:

$$S(N, M, \nu) = P(N, M).FT(ACF(N, M)) \tag{1}$$

The reduction task is designed as a stack machine using object-oriented techniques internally. It is given a recipe as part of the XML sent during the CONFIGURE action (Lightfoot et al. 2000). The reduction system creates a real time gridder image for quick-look image and spectral displays, and for focus and pointing calculations.

Depending on the observing mode (see below), the relevant sky reference power ($S_{off}(M)$) is subtracted and divided out of each on-source sample power ($S_{on}(N, M)$) to remove the system band-pass response, and the result calibrated by $T_{sys}(M, \nu)$:

$$T_A^*(N, M, \nu) = T_{sys}(M, \nu) \cdot \frac{S_{on}(N, M, \nu) - S_{off}(M, \nu)}{S_{off}(M, \nu)} \tag{2}$$

The result is a calibrated spectrum for each sample and each

Table 2. ACSIS bandwidth/resolution configurations allowable with HARP.

Nominal bandwidth	Usable bandwidth /MHz	No. of sub-bands	Spectral channels per sub-band	Channel spacing /kHz	Notes
250 MHz	~220	1	8192	30.5	
500 MHz	~440	1	8192	61.0	Hybrid configuration
1 GHz	~930	1	2048	488.3	
2 GHz	~1860	1	2048	976.6	Hybrid configuration
250 MHz	~220	2	4096	61.0	
1 GHz	~930	2	1024	976.6	

DCM, $T_A^*(N, M, \nu)$, in units of antenna temperature (Kutner & Ulich 1981). This includes the full header information with sky coordinates and other relevant data. These spectral data are saved to disk using a dedicated computer and task. The maximum sustainable data rate is limited by the disk access time on this computer. Currently this is 1-2 MBytes s^{-1} , which is equivalent to a sample time of 100 ms using HARP in the 1 GHz/2048 channel configuration.

The time-series data are processed using the ORAC Data Reduction Pipeline (ORAC-DR, Cavanagh et al. 2008), creating data-cubes from all the observing modes where appropriate, co-adding multiple observations to cover larger areas of the sky or to improve signal-to-noise, and performing quality assurance tests. This pipeline runs at the summit and also off-line using enhanced data reduction recipes. The pipeline automatically determines baseline regions, by analysing the data-cubes and looking for lines using the CUPID application (Berry et al. 2007) and the Starlink KAPPA MFITREND application (Currie et al. 2008) and uses this knowledge to calculate high-quality integrated intensity images and velocity maps. There are data reduction recipes tuned for narrow-line sources, sources with densely packed lines and also broad-line sources. The time-series and processed data are archived at the Canadian Astronomy Data Centre (CADC) and are made available through the JCMT Science Archive (Economou et al. 2008).

3.3.1 Calibration

In addition to reducing the on-sky data, reduction recipes have been written to create the $T_{sys}(M, \nu)$ data used for calibration. These recognize flags on the input stream from the Sync task as being samples taken on the frontend calibration loads or sky calibration.

3.4 Control systems - RTS, JOS and the observatory control system

The real time aspects of data-taking are under control of the RTS. The RTS is hard-wired to the subsystems throughout the observatory using a 3-wire handshaking system, operating with submillisecond response times. An observation (for example, a scan map, Sec. 4.1) is a recipe consisting of several real time sequences of data-taking. During each of the sequences, the RTS controls the data-taking, i.e. starting and stopping each integration or sample in the correlator and TP detectors, by asserting and de-asserting flags over this cable in real time, under the control of a clock within the RTS. Each individual integration or sample is assigned a unique sequence number (N), which tags the data taken at that time. The TCS also assigns coordinates for each sequence number, which allows the off-line reduction system to determine the coordinates of

that data and, for example, to create a data-cube or map in sky coordinates. A typical sequence during a scan map might be a single scan of the telescope across the sky, or an integration on the sky reference position or calibration load. In most cases, the start of a sequence in the RTS is triggered by a telescope ‘on-source’ flag being asserted; this on-source flag is one of the inputs to the RTS.

The non time-critical aspects of observatory control, i.e. the setup of the subsystems before the start of each sequence, is under control of the JCMT Observation recipe Sequencer (JOS; see Kackley et al. 2004; Rees et al. 2002). This is a high-level control system which executes the observing recipe, setting up the many sequences within each recipe. It has a GUI to allow the user to monitor progress and subsystem status within the recipes, and to start, pause or abort observations. The observing recipe is written in Perl, and the subsystem configuration files are written in XML. The combination of the recipe and the subsystem configuration files gives a complete description of the observation.

The control system for HARP is implemented at several different levels. The JCMT Observatory Control System (OCS) controls HARP through a series of DRAMA actions that have been standardized for all frontends at the JCMT. The four key commands are INITIALIZE, CONFIGURE, SETUP_SEQUENCE, and SEQUENCE. The INITIALIZE action is used primarily at the start of an observing session to bring the receiver into a known passive state. The CONFIGURE action tunes the receiver to a new frequency. SETUP_SEQUENCE prepares the receiver to start an integration, setting the optics to direct the beam to the sky or to a particular thermal load. The SEQUENCE command locks out mechanical changes to the receiver while the backend is taking data.

The OCS commands to tune HARP are passed to the dedicated HARP microcomputer, which is a Power-PC based embedded system running the VxWorks real-time operating system. It receives high-level software commands from the OCS and other telescope subsystems through the DRAMA messaging facility over a standard Ethernet connection. The HARP microcomputer then communicates with the low-level HARP control electronics via a Controller Area Network (CAN) bus.

A single observation is known as a Minimum Schedulable Block (MSB). It is written in XML and is a high-level description of the observation, including the required observing recipe. At the highest level, the MSB is normally written using the JCMT Observing Tool (OT), which forms the interface between the user and the system (Folger et al. 2002). The MSB is a time-independent and system-independent description of the observation – i.e. it does not matter when the observation is actually performed, or how the system is actually cabled at the time of execution. To convert from the MSB to the real recipe at runtime, a task known as the translator writes XML configuration files that the JOS sends to all the subsystems to tell them the configuration for the observation. The

translator also writes a JOS configuration file (also XML), which tells the JOS the recipe name, as well as recipe parameters like the step time, minimum number of integration steps, etc.

4 OBSERVING MODES

There are many possible observing modes using ACSIS and the heterodyne frontends, each of which is a combination of mapping method, switching method and stepping method. The main mapping methods are scan, jiggle and stare. The switching methods are: ‘nod’ in which the telescope is moved, ‘chop’ in which the secondary mirror is moved and ‘frequency switch’ in which the LO moves. The stepping methods are ‘sample’ for a single observation and ‘grid’ for a regular grid or user-defined pattern. Additionally, there are (or are planned) modes which allow skydips, flat-fielding and calibration.

For HARP, the standard ‘fiducial’ receptor is chosen from one of the four centre receptors, and appears in the centre of the source when the telescope offsets are zeroed out. This receptor is used for pointing and focus observations.

A ‘stare’, or sample observation with HARP is a sparse map covering $\sim 100 \times 100$ arcsec, with 16 positions spaced at 30 arcsec. The receptors are labelled by the reduction software from H00 to H15, and the position of each detector on the sky is dependent upon the orientation of the array, which depends on a combination of the K-mirror and the source hour angle/elevation. An image of a single position-switch stare observation, often used for source calibrations, is shown in Fig. 16 (top) with the receptors labelled. In this observation, receptors H00 and H03 were turned off, and the pixel size has been specified in the data reduction as 15 arcsec. In sample observations, the sky reference position can be obtained using a position switch, as in this case, or using a chop (also called beam-switch). The spectra from each position are shown in Fig. 16 (bottom), where emission from the compact source is only seen with detector H06.

Only the highest-priority observing modes have been, or are shortly expected to be, implemented, and these are described below.

4.1 Mapping large fields

For mapping large areas, the scanning technique is used. This technique is also known as on-the-fly mapping, or rastering. This mode requires the highest-performance levels from ACSIS, and is used to produce fully-sampled rectangular maps of large areas. The most common method is to cover the whole map as rapidly as possible, and then to co-add multiple maps to increase the signal-to-noise ratio. This reduces effects caused by slow sky transmission variations, pointing changes or calibration drifts. The relative calibration uncertainties across maps are minimized in this way.

In the scanning observing mode, the telescope is moved steadily across the source while the data are integrated and dumped continuously, up to a maximum rate of once every 100 ms. The K-mirror is used to rotate the array at an angle of 14.48 deg with respect to the scan direction, which sets the sample spacing perpendicular to the scan direction to be 7.3 arcsec. For HARP/ACSIS at the JCMT, the scan direction reverses for each consecutive row of the scan. Fig. 17 is a schematic diagram of a scan in progress, showing the 16 HARP receptors scanning along a row on a grid of map pixels.

The rectangular map to be observed can be rotated using an

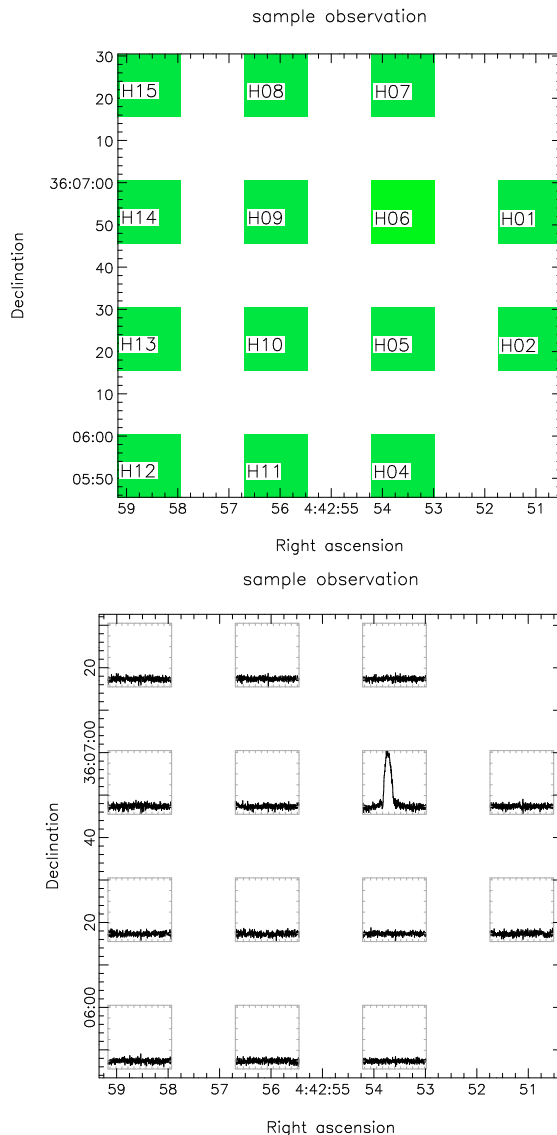


Figure 16. Grid-position-switch stare observation, with receptors labelled. H00 and H03 have been turned off (top). The spectra from each position in the image (bottom).

area position angle in the OT, with an appropriate scan position angle so that areas can be observed at any orientation. Effectively, the largest single map that can be made is 1 square degree. The telescope is nodded to the off-source reference position at the end of one or more rows, where the default number of rows is specified by the observatory. The off position is a single, specified reference position, observed in stare mode, which observes simultaneously an off position for each receptor. The off position can be specified in absolute or relative co-ordinates, and can also be specified in a different co-ordinate system than for the target. A linear combination of the two nearest (in time) applicable off-source reference observations are used with each individual on-source sample, and with the nearest (in time) calibration information to form a fully-calibrated spectrum for each sampling position of the array. The off-source integration time is a factor f greater than the length of the individual scanning sample time, so that when combined with the ‘on’ observations it gives optimum signal-to-noise ratio on the map. $f = t\sqrt{N}$, where N is the number of sample points per row,

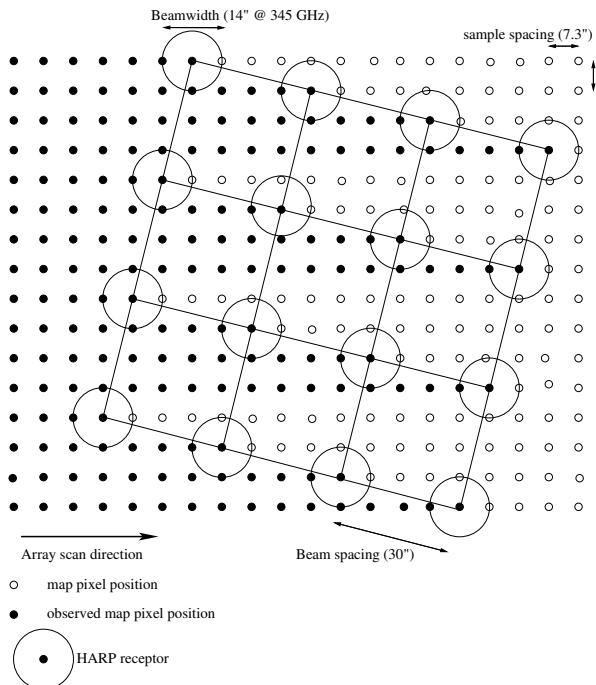


Figure 17. Schematic diagram of a scan observation.

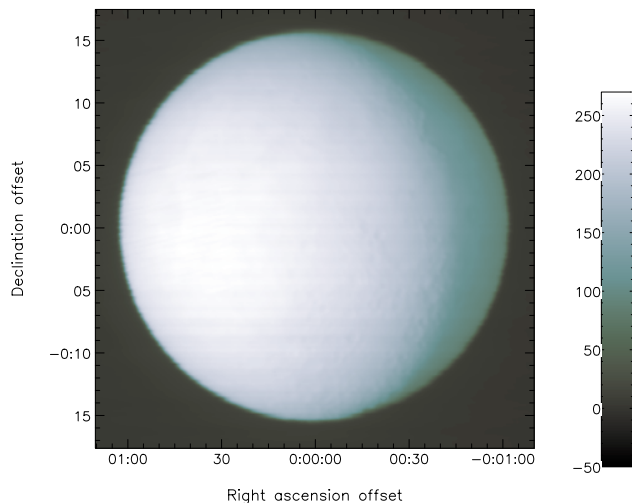


Figure 18. Scan observation of a nearly full Moon at 345.79 GHz.

and t is the sample time. The noise in a single scan does vary due to the change in effective integration time when using an interpolated off.

A basket-weave technique is normally used with scanning modes in order to minimize the effects of sky and system uncertainties in a map. This technique scans in different directions for each map, so that different receptors are used to sample the same sky point, thus reducing the effects of inaccurate flat-fielding and noisy or non-working receptors. The optimum change is a 90-degree rotation of the scan direction, which can be set in the OT.

Fig. 18 shows a 2100×2100 arcsec scanning observation of a nearly full Moon at 345.79 GHz, taken during commissioning in December 2006.

4.2 Mapping small fields

In order to map regions smaller than 2×2 arcmin, jiggle or grid observations can be carried out.

The jiggle-chop (also known as beam-switch) observing mode should be used for mapping fields smaller than the array field of view where there are emission-free positions within 180 arcsec of the source. This is the most efficient observing technique for a fully-sampled map using an array receiver, since it requires only small movements of the secondary mirror.

In this mode, the secondary mirror is moved to observe a regular grid-pattern of points on the sky (the jiggle), and then moves off the source to obtain the sky reference (the chop). The telescope is also moved to put the source in the opposite beam (a nod) so that half of the observations are done at a sky position on one side of the source, the other half at a sky position on the opposite side. This reduces systematics arising from the secondary chopping to one direction on the sky.

There are two different methods of centring the source within the map. A receptor-centred jiggle pattern will align the fiducial receptor with the source, and produce a map that is asymmetric around the target position. Since the orientation of the map is determined by the K-mirror rotation, it is not possible to specify the direction of the asymmetry, and only the central 1.5×1.5 arcmin is guaranteed to be mapped. This is a consequence of HARP having a 4×4 grid layout with no central receptor.

To fully sample the footprint of the array, special jiggle patterns called HARP4 and HARP5 have been implemented at the JCMT. HARP4 produces a 16-point rectangular map with 7.5 arcsec spacing (i.e. slightly under-sampled), while HARP5 produces a 20-point rectangular map with 6 arcsec spacing, which is slightly over-sampled with respect to Nyquist sampling of the nominal beam at 345 GHz. Both of the maps will cover a region of 2×2 arcmin. These two jiggle patterns can be specified as either pixel-centred, where the source falls in one of the central four map pixels, creating a slightly asymmetric map; or map-centred, where the source centre is between the four pixels at the centre of the map. HARP4 and HARP5 patterns can be used to fill in the under-sampling of the array on the sky, and produce fully-sampled maps. Other jiggle patterns, such as 3×3 or 11×11 can be used to produce under- or over-sampled maps. Fig. 19 shows HARP4 and HARP5 jiggle observations in $^{12}\text{CO } J = 3 \rightarrow 2$ emission of an extended source towards Serpens, taken during science verification observations for the JCMT legacy surveys. Both of these maps show similar spatial and spectral structures, and, as expected, have integrated intensities and standard deviations across the image that differ by less than the variations due to changing observing conditions, such as source elevation and weather. The HARP4 datacube has a lower noise per pixel than the HARP5 datacube.

The jiggle position-switch observing mode is a similar technique, which can be used for sources where the emission-free region is relatively far away from the source. In this case, the secondary mirror is jiggled as described above to observe the source, but the telescope is moved (a position-switch) to observe the off position. A grid observing mode is also available. The grid position-switch moves the telescope to each position in a user supplied grid and executes a stare observation. The grid pattern is supplied in arcsecond offsets, and can be any shape or size. All of the chop and position-switch modes can be used to carry out sample observations, in which case only a single point for each receptor is observed, and a sparse map such as that shown in Fig. 16 is produced. For all of the jiggle patterns, and for the grid observing mode, ei-

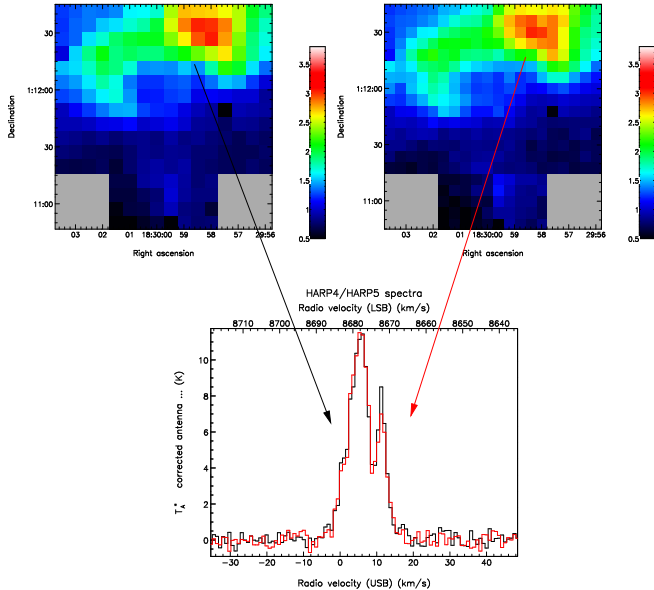


Figure 19. Integrated intensity maps of jiggle position-switch observations in $^{12}\text{CO } 3\rightarrow 2$ towards a region in Serpens, utilizing the HARP4 pattern (left) and HARP5 pattern (right). Detectors H00 and H03 have been turned off. Spectra from the same spatial position near the peak are also shown, in a linestyle matching the arrow to the full map (bottom).

ther shared off-source reference positions, defined in the same way as for scans, or separate off positions for each position in the jiggle pattern can be used. The off position can be specified in the same way as for scan modes. The choice between these two depends upon the observing mode, the integration time, and how much spatial smoothing will be required in the data analysis. The choice is a compromise between efficiency and photometric accuracy, since the noise in observations with shared off-source reference positions will be correlated.

4.3 Frequency switching

The majority of the observing modes mentioned above will be available in frequency-switched mode, which is being implemented for jiggle maps in 2009. In frequency switching with HARP and ACSIS, the switching rate must generally be faster than the scanning rate. In laboratory testing, HARP is able to switch at a rate < 1 ms, for a step size up to 50 MHz.

5 SYSTEM CHARACTERISATION OBSERVATIONS

5.1 Beam measurements and efficiencies

HARP5 jiggle-chop observations of Saturn, with 6 arcsec map pixels, were carried out in order to determine the beam efficiencies for each receptor. The observations were made at 345 GHz, and the calculations were carried out using data on Saturn from the JCMT FLUXES programme, with Saturn at a diameter of 19.48 arcsec, and having a brightness temperature of 116.02 K at the time of the observations. Moon efficiency observations were also carried out at three frequencies, through sample observations on the full Moon. The Moon efficiency calculations were made following Mangum (1993). The results from these calculations are listed in Table 3. The

Table 3. HARP efficiencies for Saturn (η_{mb}) and the Moon (η_{fss}), measured on 4th/5th February, 2007.

Receptor	η_{mb}	η_{fss}		
	345 GHz	330 GHz	345 GHz	360 GHz
H01	0.58	0.70	0.74	0.73
H04	0.64	0.74	0.78	0.77
H05	0.64	0.71	0.77	0.76
H06	0.62	0.71	0.76	0.75
H07	0.58	0.68	0.75	0.71
H08	0.58	0.68	0.78	0.75
H09	0.63	0.72	0.78	0.77
H10	0.63	0.74	0.78	0.77
H11	0.58	0.69	0.78	0.76
H12	0.61	0.73	0.78	0.77
H13	0.62	0.77	0.79	0.78
H14	0.58	0.74	0.78	0.77
H15	0.57	0.74	0.78	0.78

Table 4. HARP single sideband receiver temperatures.

Receptor	Receiver Temperature (K)				
	328 GHz	340 GHz	350 GHz	360 GHz	370 GHz
H01	123	110	110	105	181
H04	133	85	96	100	162
H05	165	82	93	87	127
H06	117	140	91	84	114
H07	155	122	116	103	165
H08	148	93	93	97	147
H09	190	125	134	122	189
H10	97	150	87	84	122
H11	120	145	105	92	143
H12	245	123	123	115	133
H13	119	140	91	90	103
H14	99	144	95	86	116
H15	132	152	100	89	106

numbers are similar to those measured for the previous 350 GHz receiver at the JCMT, RxB3i. Current and archived measurements of efficiencies and receiver temperatures (Sec. 5.2) are available from the JCMT web site.¹

5.2 System sensitivity and stability

The performance of HARP’s receptors exceeds the specification for receiver temperature (T_{rx}) by a large margin. The original specification covered just the central 20 GHz of the tunable range, with the ratio $T_{\text{rx}}/\eta_{\text{mb}} < 330\text{K SSB}$. Receiver temperatures were measured using a nitrogen bucket in the receiver cabin in place of the cold load. Measurements were taken at several local oscillator frequencies across the tunable band, and are listed for each working receptor in Table 4. Across the tunable range, the variation in effective system temperature for each receptor is less than 15 per cent. Current receiver temperature measurements are listed on the JCMT web site.

¹ http://www.jach.hawaii.edu/JCMT/spectral_line/

Table 5. Lower limits on sideband rejection.

Receptor	Rejection (dB)		
	356 GHz	354 GHz	345 GHz
H00			>17.86
H01			>17.86
H02			>17.86
H03			>17.86
H04	>21.84	>15.73	>17.98
H05	>25.09	>37.31	>17.77
H06		>15.88	>40.48
H07	>20.56		
H08		>18.97	>16.02
H09	>17.00	>16.11	>16.39
H10	>30.98	>29.91	>27.21
H11	>18.25		>21.43
H12	>28.61	>15.03	>24.45
H13	>17.91	>17.19	>40.66
H14	>22.40	>19.14	>17.16
H15		>27.02	>20.20

5.3 Sideband rejection

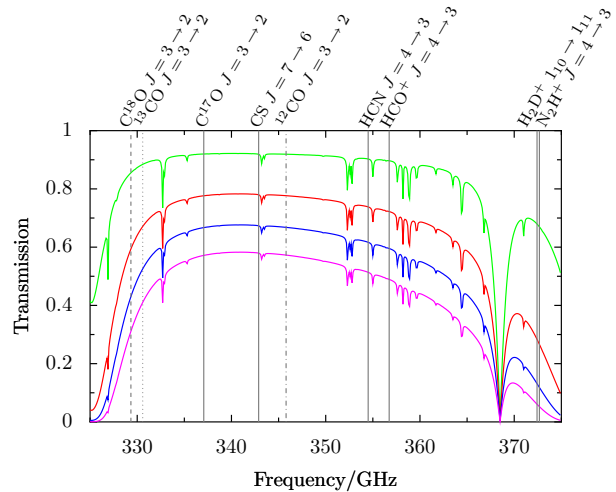
On-sky observations were made at several different frequencies towards sources known to have strong emission lines. In most cases, since the line was not detected in the image sideband, we can only give lower limits to the rejection. For a few of the detectors, excess noise in the spectrum meant that the ratio could not be calculated. Table 5 lists the lower limits on sideband rejection in dB for each detector at several central frequencies. On average, and across the tuning range, the sideband rejection is better than 19 dB.

5.4 Calibration

Much work has been done on characterizing and improving the new spectral imaging system. This is a complex task, since the system is composed of a frontend, backend and K-mirror, all of which are newly-commissioned, plus telescope upgrades, and newly-written telescope, data acquisition, and data reduction software. For the integrated systems at the JCMT, under good conditions, and assuming pointing and focus are good, the uncertainties associated with calibrational accuracy of any of the spectral frontends combine to a total of ~ 20 per cent. The factors contributing to this are explained in full on the JCMT web page.² For the new spectral imaging system, a review of the calibration observations taken for the Gould Belt Survey (Ward-Thompson et al. 2007) show HARP intensity values (mostly) below the reported JCMT standard values by up to 23 per cent, with a mean difference of 15 per cent, for calibration observations taken at 345 GHz, 329 GHz and 330 GHz.

6 SCIENTIFIC OBSERVATIONS

HARP and ACSIS provide simultaneous mapping and high-resolution spectroscopy with high sensitivity in the 325 to 375 GHz (850 μm) band. The spatial dimension of these maps is well matched to continuum images obtained with SCUBA, and which will be obtained with SCUBA-2. The spectral dimension of the HARP/ACSIS maps provides far more information than can be obtained with continuum images. In this section, we describe some of

**Figure 20.** Atmospheric transmission for several different amounts of water vapour at the JCMT in the HARP observing range, corresponding to JCMT weather bands 1 to 4. Astrophysically important lines are marked.**Table 6.** Some of the important molecular lines observable with HARP. Examples of lines which can be observed simultaneously have been listed in pairs.

Transition	Frequency /GHz
C ¹⁸ O/ ¹³ CO 3→2	329.330/330.587
C ¹⁷ O 3→2/C ³⁴ S 7→6	337.061/337.396
CH ₃ OH 7 ₁₄ → 6 ₁₄	338.345
CS 7 → 6	342.883
H ¹³ CN 4 → 3	345.340
CO 3 → 2	345.795
H ¹³ CO ⁺ 4 → 3/SiO 8 → 7	346.999/347.330
HCN 4 → 3	354.505
HCO ⁺ 4 → 3	356.734
DCN/HNC 4 → 3	362.046/362.630
H ₂ CO 5 ₀₅ → 4 ₀₄	362.736
H ₂ D ⁺ 1 ₁₀ → 1 ₁₁ /N ₂ H ⁺ 4 → 3	372.421/372.672

the first science observations taken with the new system as part of the HARP/ACSIS instrument teams guaranteed time.

Comparisons of different lines enables the temperature, space density and composition of the gas to be derived, all of which are essential in understanding the underlying astrophysical processes. The molecular transitions available in the HARP frequency range trace moderate density (10^3 to 10^7 cm^{-3}) and temperature (10 to 100 K) regimes, probing the warmer, more excited gas associated with energetic events such as star formation. With the instrument placed at the JCMT on Mauna Kea, the atmospheric transmission allows sufficiently dry nights to obtain good sensitivity at the edges of the band, where astrophysically important transitions from molecules such as C¹⁸O and N₂H⁺ lie. Fig. 20 shows the position of these lines, along with the atmospheric transmission across the frequency range. Table 6 lists a sample of the lines observable with HARP, and Fig. 21 shows a wideband spectrum at 345 GHz taken towards OMC1, where many lines can be observed.

² http://docs.jach.hawaii.edu/JCMT/HET/GUIDE/het_guide/

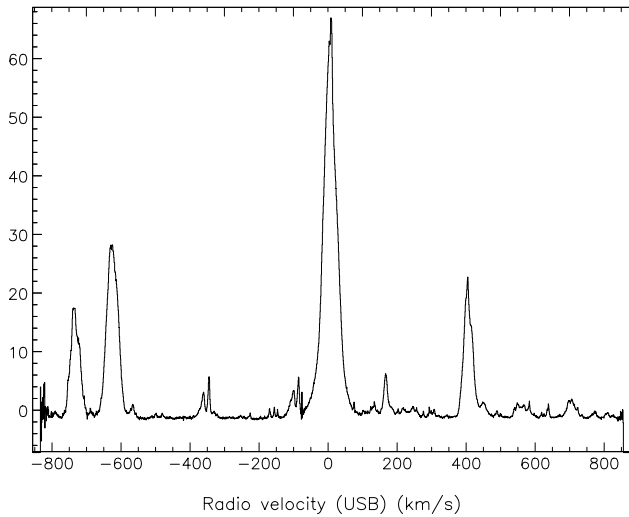


Figure 21. Wideband spectrum ($\Delta v=1.9$ GHz) at 345 GHz towards OMC1, showing the wealth of lines observable in this frequency range, observable in a single tuning.

6.1 Large-scale mapping of molecular clouds

6.1.1 Perseus

Mapping the kinematics of star formation can provide crucial discriminators between models of star formation. As part of the HARP guaranteed-time programme of observations we surveyed gas kinematics in the CO, C¹⁸O and ¹³CO $J=3 \rightarrow 2$ spectral lines across a wide region of the Perseus molecular cloud (Curtis, Richer & Buckle 2009). These three tracers are a powerful diagnostic tool in understanding star-forming regions and will be extensively utilized in the forthcoming Gould Belt Legacy Survey (Ward-Thompson et al. 2007). Of particular importance for the Legacy Survey is the multiple sub-band mode, where C¹⁸O and ¹³CO $3 \rightarrow 2$ can be observed simultaneously, and CO can be observed in a high resolution/narrow band mode simultaneously with a medium resolution/wide band mode. One of the mapped regions in the east of Perseus, IC348, is shown in the different isotopologues in Fig. 22. All of these data took just 12 hours to collect, compared to the roughly 4 weeks expected with the previous B-band receiver on JCMT. The region is a dense molecular ridge of about $200 M_{\odot}$, some 10 arcmin to the south-west of the IR cluster IC348 itself. The centre of the cluster is almost devoid of star-forming activity (Luhman et al. 1998) in contrast to this ridge which contains numerous sites of low-mass star formation (Walawender et al. 2006). It notably contains the well-studied extremely collimated young outflow, HH211 (clear in the CO maps as the dumbbell shaped object, Fig. 22). Discovered by McCaughrean, Rayner & Zinnecker (1994), it is the best example of a molecular *jet*, with intense molecular beams terminating in H₂ bow-shocks (e.g. Chandler & Richer 2001).

When used in combination with SCUBA dust continuum maps, the HARP data offer powerful insights into the velocity structure of the regions and optical depths. The optically thin C¹⁸O traces the velocity structure in and around the dense cores, identified in SCUBA maps (Hatchell et al. 2005, 2007) which can be used to explore the turbulent environment just outside of the cores. The total intensity traces the dust very accurately and individual star-forming cores may be differentiated. The ¹³CO data probe the bulk motions of the cloud and trace the highest-density protostellar

outflows. Numerous cavities and clumps are clear, which may be relics of a previous generation of star-forming objects (e.g. Quillen et al. 2005). Finally, the ¹²CO data trace mainly high-velocity outflows, which may regulate the whole process by feeding-in large quantities of energy and momentum into the cloud bulk (Norman & Silk 1980; Li & Nakamura 2006). In this region three or four outflows are clear, totalling some 1.2×10^{37} J of kinetic energy which is close to the cloud's turbulent energy, 2.7×10^{37} J, suggesting the possible link between outflows and cloud turbulence.

6.1.2 Orion

The guaranteed time observations carried out jointly between the HARP and ACIS teams observed 2.7 deg^2 of the Orion A molecular cloud in ¹²CO $J=3 \rightarrow 2$. This region contains the L1641 cloud and the integral filament (with OMC1), allowing study of both extremely bright (OMC1 and L1641N) and more quiescent regions (further south). The scientific analysis being carried out is primarily aimed at producing a census of protostellar outflows in the region. Currently these outflows are being identified and characterized with respect to their energy, momentum and mass, whilst investigating their effect on the cloud as a whole. Our ¹²CO observations allow an estimate of the mass of the whole cloud, which places a lower limit on the mass contained in the region observed here of $10^3 M_{\odot}$. This accords well with Bally et al. (1987) who found a mass of around $5 \times 10^4 M_{\odot}$ in an area over twice as large (8 deg^2 compared with 2.7 deg^2) observed in a less optically thick tracer (¹³CO $J=1 \rightarrow 0$).

Fig. 23 shows some of the strongly red- and blue-shifted gas located in the integral filament as a red-green-blue false-colour image. Fig. 24 shows an integrated intensity map from a more southerly region (below L1641N). Although the gas here is less bright and more quiescent, Fig. 24 clearly shows some exciting jet-like structures. Some of these are associated with HH objects, such as HH 43 in the current image. The bright clump of emission is at the position of HH 43 – which also appears as a strong knot when observed in infrared $2.12 \mu\text{m}$ H₂ data in Stanke, McCaughrean & Zinnecker (2000, 2002). The fainter collimated tail extending NW aligns well with the short flows SMZ68 (identified as a bow shock in Stanke et al. 2002) and the longer SMZ67, a giant flow identified from a number of knots between HH 43, 38 and 64, and extending considerably further than the visible ‘tail’ seen in CO. The giant H₂ flow has a length of 1.45 pc, compared with approximately 0.7 pc, or 5 arcmin in CO. Their predicted driving source for the giant flow is at a position just at the NW end of the tail seen in CO.

6.2 High resolution spectral imaging of protostellar cores

Finally, we have carried out a direct comparison of observations towards a protostellar core in IC 5146, undertaken with HARP and with RxB3i. Fig. 25 shows the spectra of C¹⁸O $J=3 \rightarrow 2$ taken with the two instruments at a single position, and the integrated intensity image, obtained with RxB3i, overlaid with contours from observations obtained with HARP. The RxB3i observations fully-sampled a region 180×200 arcsec in size, and took 10 hours of observing time. The HARP observations fully-sampled a region 1300×200 arcsec in size, and took 2.5 hours of observing time. The correspondence between the two sets of observations is consistently good both spatially and spectrally.

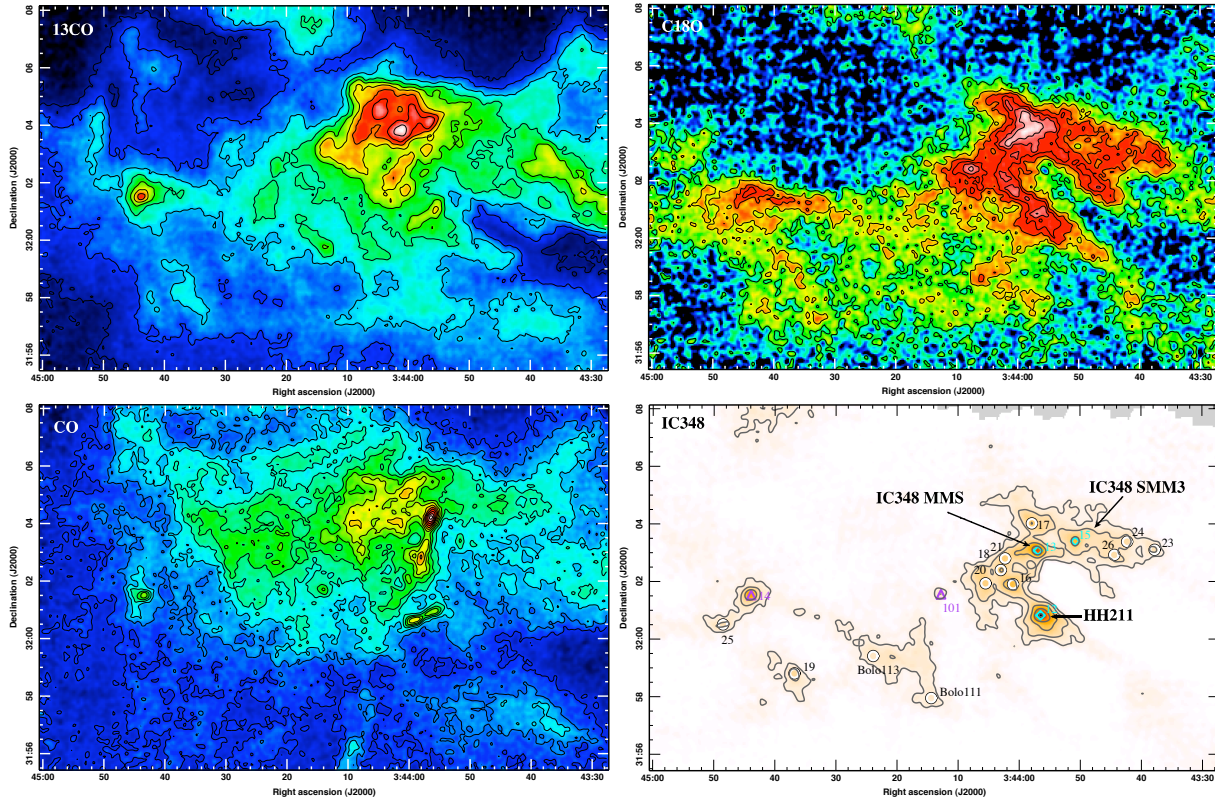


Figure 22. HARP ^{13}CO (top left), C^{18}O (top right) and ^{12}CO (bottom left) $J = 3 \rightarrow 2$ integrated intensity images towards IC348 taken as part of the guaranteed time. For comparison a SCUBA 850 μm dust emission map is also show (bottom right, Hatchell et al. 2005), with cores classified by Hatchell et al. (2007), and marked as starless (black and white circles), Class 0 (blue diamonds) or Class I protostars (purple triangles). The optically thin C^{18}O map closely follows the compact SCUBA emission, although there are some differences, while the ^{13}CO traces the bulk of the ambient cloud. By contrast the ^{12}CO map is dominated by the emission from young protostars in the region, notably HH211 (the northwest-southeast oriented ‘dumbbell’ at $03^{\text{h}}27^{\text{m}}39^{\text{s}}, +30^{\circ}13'00''$) and IC348-MMS (the nearly north-south oriented flow centred at $03^{\text{h}}27^{\text{m}}43^{\text{s}}, +30^{\circ}12'28''$)

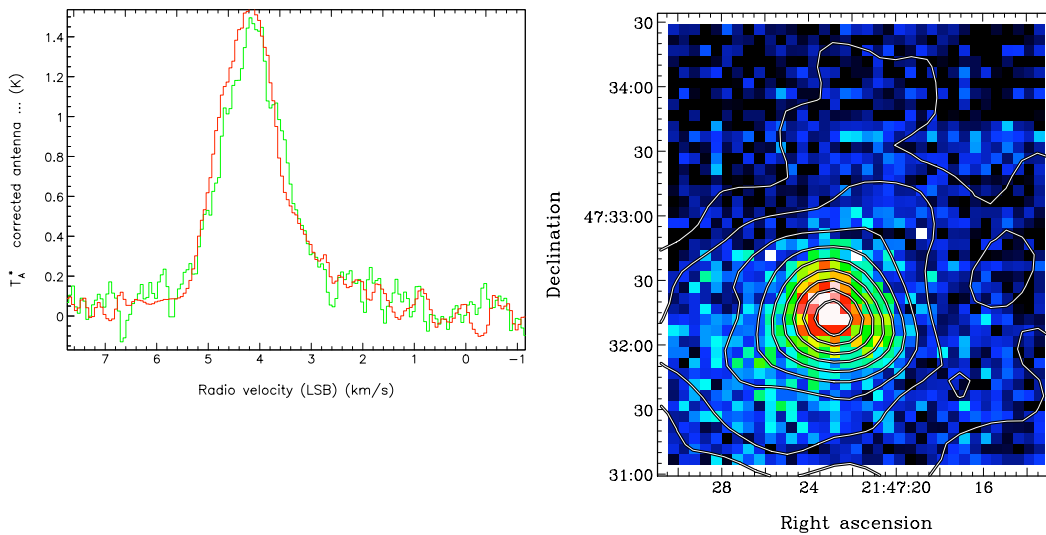


Figure 25. Left: Comparison of peak spectra for eastern core of IC5146. with Rx B3 in red and HARP in green. Right: Comparison of the HARP data (contours) with the previous receiver B3 observation (colour scale) of the eastern core of IC5146 in C^{18}O $J = 3 \rightarrow 2$. The contour levels levels are of 0.25, 0.50, ... 2.25 K km/s.

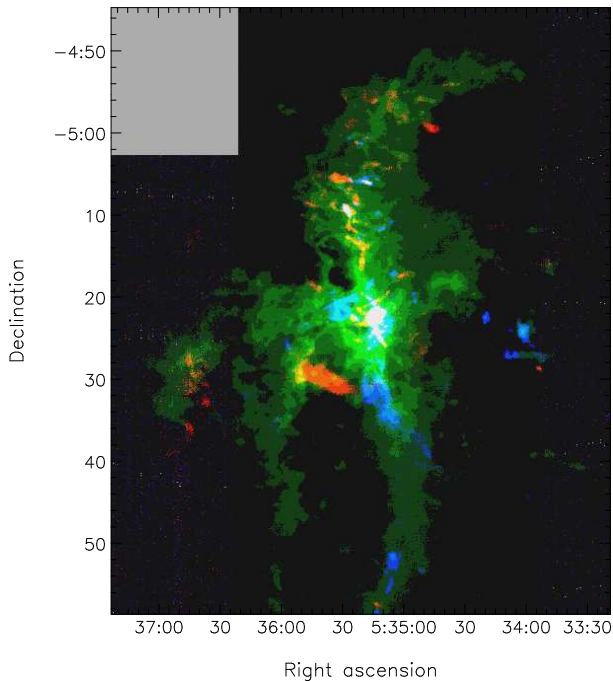


Figure 23. The Orion filament, integrated from -0.9 to 17.1 km s^{-1} (green), 14.1 to 34.1 km s^{-1} (red) and -14.8 to 5.1 km s^{-1} (blue) shown as an rgb false colour image.

7 SUMMARY

We have presented details of a new submillimetre spectral imaging system that has been installed and commissioned on the JCMT. HARP is a 16-element focal plane array receiver which operates from 325–375 GHz. Receiver temperatures are $\sim 120 \text{ K}$ and under good weather conditions system temperatures are $\sim 300 \text{ K}$ (SSB) at 345 GHz. At 345 GHz $\eta_{\text{mb}} = 0.61$, measured in 2007. A polarising Mach-Zehnder interferometer is used for sideband separation, and sideband rejection is better than 19 dB. HARP operates in conjunction with ACSIS, which offers versatile bandwidth and spectral resolution configurations for all of the JCMT heterodyne receivers. In addition, ACSIS provides configurations that allow simultaneous observations of multiple lines, which can have different bandwidth and resolution configurations.

With HARP and ACSIS, the widest bandwidth available is 1.9 GHz with a channel spacing of 0.977 MHz, while the highest spectral resolution mode has a channel spacing of 31 kHz, or 0.03 km s^{-1} , with a bandwidth of 220 MHz. Since HARP is an array receiver, mapping speeds are increased, and it is possible to make fully-sampled maps of 1 square degree in less than 1 hour. A direct comparison between HARP and the previous JCMT single-pixel receiver RxB3i showed HARP observations mapping the region 28 times faster.

HARP and ACSIS provide simultaneous mapping and high resolution spectroscopy with high sensitivity, and with spatial dimensions well-matched to continuum images obtained with SCUBA. There are a wide range of scientific galactic and extragalactic projects being carried out using this system at the JCMT. We presented some of the first science observations carried out as part of the HARP/AC SIS guaranteed time for the instrument teams, and highlighted the importance of observations using the new spectral imaging system in understanding astrophysical processes.

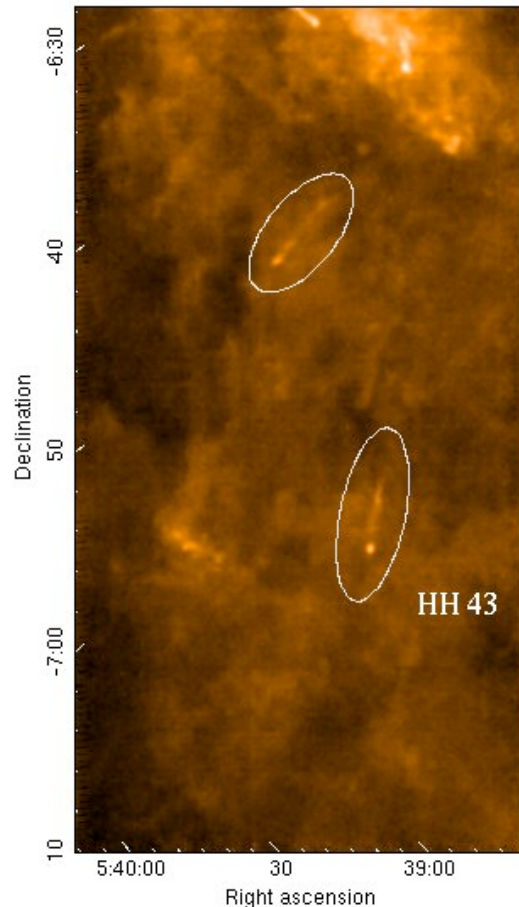


Figure 24. A region from the Orion A HARP/AC SIS GT survey. Two prominent jet-like structures are highlighted. Both contain a bright knot-like ‘nose’ with a fainter ‘tail’ streaming away. The lower one is at the position of the Herbig–Haro object HH 43.

ACKNOWLEDGMENTS

The Cavendish Astrophysics Group would like to acknowledge the technical expertise of P. Doherty, V. Quy and H. Stevenson in the building of HARP. The authors would like to thank the referee, Gary Fuller, for helpful comments and suggestions. The James Clerk Maxwell Telescope is operated by The Joint Astronomy Centre on behalf of the Science and Technology Facilities Council of the United Kingdom, the Netherlands Organisation for Scientific Research, and the National Research Council of Canada.

REFERENCES

- Bailey J.A., Farrell T., Shorridge K., 1995, in Wallace P.T., eds, Proc. SPIE Vol.2479, DRAMA: an environment for distributed instrumentation software, SPIE, p.62
- Bally J., Stark A.A., Wilson R.W., Langer W. 1987, ApJ, 312, L45
- Bell G.S., 2008, PhD thesis, Univ. Cambridge
- Berry D.S., Reinhold K., Jenness T., Economou F., 2007, in Shaw R.A., Hill F., Bell D.J., eds, ASP Conf. Ser. Vol. 376, Astron. Data Analysis Software and Systems XVI p. 425

- Cavanagh B., Jenness T., Economou F., Currie, M. J., 2008, *Astron. Nachrichten*, 329, 295
- Chandler C.J., Richer J.S., 2001, *ApJ*, 555, 139
- Currie, M.J., Draper, P.W., Berry D.S., Jenness T., Cavanagh B., Economou F., 2008, in Argyle R.W., Bunclark P.S., Lewis J.R., eds, *ASP Conf. Ser. Vol. 394, Astron. Data Analysis Software and Systems* p. 650
- Curtis E.I., Richer J.S., Buckle, J.V., 2009, *MNRAS* submitted
- D'Addario L.R., Thompson A.R., Schwab F.R., Granlund J., 1984, *Radio Sci.*, 19, 931
- Economou F., Jenness T., Chrysostomou A., Cavanagh B., Redman R., Berry D. S., 2008, in Argyle R.W., Bunclark P.S., Lewis J.R., eds, *ASP Conf. Ser. Vol. 394, Astron. Data Analysis Software and Systems*, p. 450
- Escoffier, 'GBT Correlator', 1998, GBT NRAO Memo 190, NRAO, Charlottesville, V.A.
- Folger M., Bridger A., Dent W., Kelly D., Adamson A., Economou F., Hirst P., Jenness T., 2002, in Bohlender D.A., Durand D., Handley T.H., eds, *ASP Conf. Ser. Vol. 281, Astron. Data Analysis Software and Systems XI*, p. 453
- Hatchell J., Richer J.S., Fuller G.A., Qualtrough C. J., Ladd, E. F., Chandler C. J., 2005, *A&A*, 440, 151
- Hatchell J., Fuller G.A., Richer J.S., Harries T. J., Ladd E. F., 2007, *A&A*, 468, 1009
- Holland, W.S. Robson E.I., Gear W.K, et al., 1999, *MNRAS*, 303, 659
- Holland, W.S. MacIntosh M., Fairley A., et al., 2006, in Zmuidzinas J., Holland W. S., Withington S. Duncan W.D., eds, *Proc. SPIE Vol. 6275, SCUBA-2: a 10,000-pixel submillimeter camera for the James Clerk Maxwell Telescope*, SPIE, p. 45
- Hovey G.J. Burgess T.A., Casorso R.V. et al., 2000, in Butcher H.R. ed, *Proc. SPIE Vol. 4015, New spectral line multibeam correlator system for the James Clerk Maxwell Telescope*, SPIE, p. 114
- Hovey G.J. Dewdney P. E., Redman R.O. et al., 2002, in Bohlender D.A., Durand D., Handley T.H., eds, *ASP Conf. Proc. Vol. 281, Astron. Data Software and Systems XI*, p. 355
- Jaeger S., 2008, in Argyle R.W., Bunclark P.S., Lewis J.R., eds, *ASP Conf. Ser. Vol. 394, Astron. Data Analysis Software and Systems*, p. 623
- Kackley R.D., Rees N.P., Walther C., Jenness T., 2004, in Lewis H., Raffi G. eds, *Proc. SPIE Vol. 5496, The JCMT observing queue and recipe sequencer*, SPIE p. 718
- Kooi J.W., G. Chattopadhyay G., Rice F., Zmuidzinas J., Withington S. 2001, 9th International Conf. on Terahertz Electronics, Charlottesville, Virginia
- Kutner M.L., Ulich B.L., 1981, *ApJ*, 250, 341
- Leech J., 2000, PhD thesis, Univ. Cambridge
- Levreault R.M., 1983, *ApJ*, 265, 855
- Li Z.-Y., Nakamura F., 2006, *ApJ*, 640, 187
- Lightfoot J.F., Dent W.R.F., Willis A.G., Hovey G.J., 2000, in Manset N., Veillet C., Crabtree D., eds, *ASP Conf. Proc. Vol. 216, Astron. Data Analysis Software and Systems IX*, p. 502
- Luhman K.L., Rieke G.H., Lada C.J., Lada E.A., 1998, *ApJ*, 508, 347
- Mangum J.G, 1993, *PASP*, 105, 117
- Matthews B.C., Greaves J.S., Holland W.S. et al., 2007, *PASP*, 119, 842
- McCaughrean M.J., Rayner J.T., Zinnecker H., 1994, *ApJ*, 436, 189
- Norman C., Silk J., 1980, *ApJ*, 238, 158
- Plume R. Fuller G.A., Helmich F. et al. 2007, *PASP*, 119, 102
- Quillen A.C., Thorndike S.L., Cunningham A., Frank A., Guter-muth R.A., Blackman E.G., Pipher J.L., Ridge N., 2005, *ApJ*, 632, 941
- Rees. N.P. et al., 2002, in Lewis H., ed, *Proc. SPIE Vol. 4848, JCMT observatory control system*, SPIE, p. 283
- Sandell G., Weintraub D.A., 2001, *ApJS*, 134, 115
- Smith H., Hills R.E., Withington S., et al., 2003, in Phillips T.G., Zmuidzinas J. eds, *Proc. SPIE Vol. 4855, Millimeter and Submillimeter Detectors for Astronomy*, SPIE, p. 338
- Smith H., Buckle J.V., Hills R.E., et al. 2008, in Duncan W.D., Holland W.S., Withington S., Zmuidzinas J., eds, *Proc. SPIE Vol.7020, HARP: a submillimetre heterodyne array receiver operating on the James Clerk Maxwell Telescope* p. 24
- Stanke T., McCaughrean M.J., Zinnecker H., 2000, *A&A*, 355, 639
- Stanke T., McCaughrean M.J., Zinnecker H., 2002, *A&A*, 392, 239
- Walawender J., Bally J., Kirk H., Johnstone D., Reipurth B., Aspin C., 2006, *AJ*, 132, 467
- Ward-Thompson D. Di Francesco J., Hatchell J., et al., 2007, *PASP*, 119, 855
- Williamson R., 2004, PhD thesis, Univ. Cambridge
- Wilson C.D., Warren B.E., Israel F.P., et al., 2009, *ApJ*, 693, 1736
- Withington S., Leech J., Yassin G., Isaak K.G., Jackson B.D., Gao J.R., Klapwijk T.M., 2001, *Int J. Ir MM Waves*, 22, 1305